Kovove Mater. 62 2024 111–117
DOI: 10.31577/km.2024.2.111

Study of electronic and optical properties of As-doped TiO_2 using first principles

Jihui Luo*, Yuke Zhan

College of Materials Science and Engineering, Yangtze Normal University, Chongqing, P. R. China

Received 24 January 2024, received in revised form 27 April 2024, accepted 02 May 2024

Abstract

This study utilized first-principles calculations to examine the electronic and optical properties of As-doped TiO_2. Three model structures with varying As concentrations (0, 2.08, and 4.17 %, atomic percentage) were analyzed to investigate band structure and the density of states and compare absorption spectrum, reflectivity spectrum, dielectric function, and conductivity on the (100) surface. The findings indicate that the As-4s and As-4p orbitals of As-doped TiO_2 influence the positions of the conduction band minimum and valence band maximum. Furthermore, the band gap of 4.17 % As-doped TiO_2 starts to decrease, reducing the energy required for electron transitions and enhancing absorption in the visible light range. As-doped TiO_2 demonstrates promising performance in reflectance, dielectric function, and electrical conductivity, positioning it as a favorable material for visible light photocatalysis applications.

K e y w o r d s: As-doped TiO_2, first principles, optical properties, band structure, absorption

1. Introduction

TiO_2 has important applications in the field of photocatalysis [1, 2], especially through the modification of TiO_2 using element doping, which reduces its band gap and enhances its ability to degrade organic compounds [3]. Doping elements include metallic elements [4–6], non-metallic elements [7–9], as well as dual-element doping [10, 11], among others. The photocatalytic performance of TiO_2 modified with these doping elements has been significantly improved. For example, Suwondo et al. [12] studied the band gap of Cu-doped TiO_2 and its photocatalytic activity. The results show that the band gap of Cu-doped TiO_2 can be narrowed to 2.878 eV. Moreover, the photocatalyst could be reused for up to 5 photodegradation cycles with no significant activity decrease. Bhosale et al. [13] investigated Mn-doped TiO_2 prepared by the sol-gel method. The research showed that the grain size began to decrease with an increase in the Mn doping content. Photocatalytic experiments demonstrated that the photocatalytic activity of 5 mol% Mn-doped TiO_2 is nearly four times that of pure TiO_2. Furthermore, Mn-doped TiO_2 exhibited excellent photodegradation capability for a mixture of Rhodamine B, Brilliant Green, and Methylene Blue dyes.

Arsenic (As) is situated in the 4th period and the VA group of the periodic table, with an outer electron configuration of $4s^2$ 3d $^{10}4p^3$. Several reports have been published on the research of As element doping modified semiconductor materials [14–16]. However, there is scarce research on doping As element in TiO_2, possibly due to its carcinogenic hazard.

Experiments that cannot be conducted due to their dangerous nature can be simulated through theoretical calculations. Utilizing first principles to examine the structure and properties of different materials is a secure, efficient, and precise approach compared to experiments. This approach is commonly employed to compute the optical properties and other characteristics of materials [17–20].

This work first calculated the optical properties of As-doped TiO_2 with different structures and As contents using first principles, providing a theoretical basis for the potential application of As elements in TiO_2 photocatalysis.

*Corresponding author: e-mail address: 20170128@yznu.edu.cn

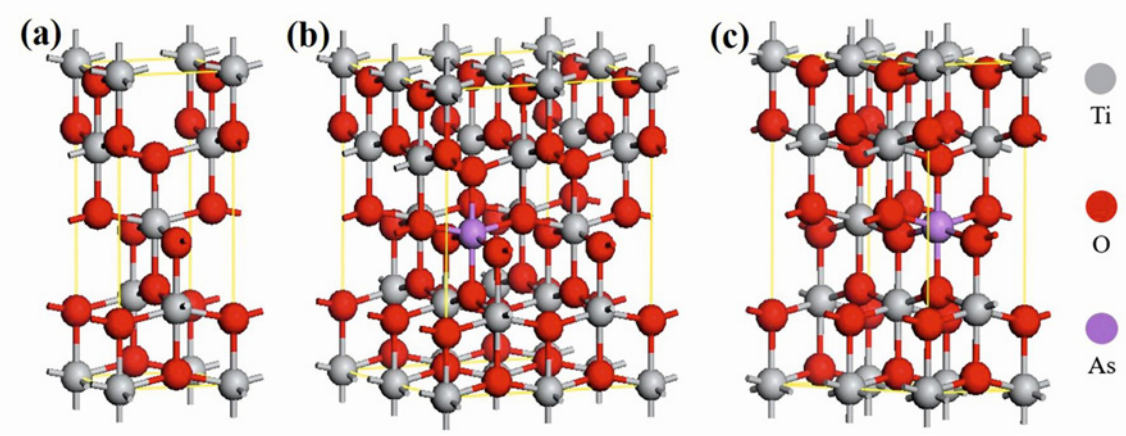

Fig. 1. Molecular models of (a) pure TiO_2, (b) 2.08 % As-doped TiO_2, and (c) 4.17 % As-doped TiO_2.

2. Computational methods

The properties of As-doped TiO_2 molecules were calculated using the CASTEP [21] module in Materials Studio 2020 software, based on the first principles of density functional theory.

First, input the unit cell of TiO_2 (Fig. 1a) and expand it into $2 \times 2 \times 1$ and $1 \times 2 \times 1$ supercell molecular structures, where O atoms are represented in red and Ti atoms in grey. Replace one Ti atom in the $2 \times 2 \times 1$ supercell with an As element to form the molecular structure model as shown in Fig. 1b. Similarly, replace one Ti atom in the $1 \times 2 \times 1$ supercell with an As element to form the molecular structure model as represented in Fig. 1c. The above three structures respectively form TiO_2 molecular models doped with As at 0, 2.08, and 4.17 % (atomic percentage). Then, structural optimization calculations will be performed using the Generalized Gradient Approximation (GGA) with the Perdew-Burke-Ernzerhof theory [22] and a cutoff energy of 380 eV.

Next, perform band structure and partial density of states (DOS) calculations on the structurally optimized molecular model. Choose the (100) surface of three different models for optical property calculations, and then compare and analyze absorption spectra, reflection spectra, loss function, dielectric function, and conductivity.

3. Results and discussion

3.1. Electronic properties

The results for pure TiO_2 indicate a band gap of 2.10 eV (Fig. 2a), which closely aligns with other calculated values of 2.12 eV [23, 24] or 2.15 eV [25]. However, this figure is lower than the experimental value of 3.2 eV, likely due to the theoretical calculation being based on idealized materials. Additionally, the GGA method used in density functional theory calculations often underestimates the band gap of metal oxides, resulting in a lower calculated band gap. Nevertheless, these deviations do not impact the relative analysis of the electronic structure. When a small amount of As element is doped, as depicted in Fig. 2b, the band gap begins to increase, reaching 2.26 eV, which is 0.16 eV higher than that of pure TiO_2. As the doping content of As increases to 4.17 %, the band gap starts to decrease again, reaching 2.07 eV (Fig. 2c), lower than that of pure TiO_2. The calculations suggest that a higher doping content of As can reduce the band gap, which is advantageous for electron transitions.

The electronic partial DOS for three different models was calculated to analyze the factors affecting the band gap. Figure 3a shows the partial DOS for the pure TiO_2 elements, where E_F represents the Fermi level. It can be observed from the figure that the valence band is mainly contributed by O-2p, while the conduction band is mainly contributed by the hybridization of O-2p and Ti-3d. A high DOS distribution at 4.53 eV is primarily contributed by the Ti-3d orbitals. The total DOS for each element is shown in the uppermost curve of Fig. 3a.

Figure 3b shows the DOS of the 2.08 % As-doped TiO_2, indicating that the valence band is still mainly influenced by O-2p orbital electrons. With the introduction of As, the minimum energy of the conduction band begins to decrease, and a high DOS distribution is observed around 1.2 eV. Compared to Fig. 3a, the DOS peak has shifted negatively by 3.33 eV. This shift occurs due to the hybridization of O-2p, Ti-3d, As-4s, and As-3p orbitals, resulting in the broadening of the conduction band bottom and leading to the negative shift of the minimum value of the conduction band. Simultaneously, the DOS in the valence band also changes, with the O-2p and Ti-3d states shifting to the left, moving away from the E_F. Although the minimum of the conduction band begins to approach the E_F, the difference between the maximum

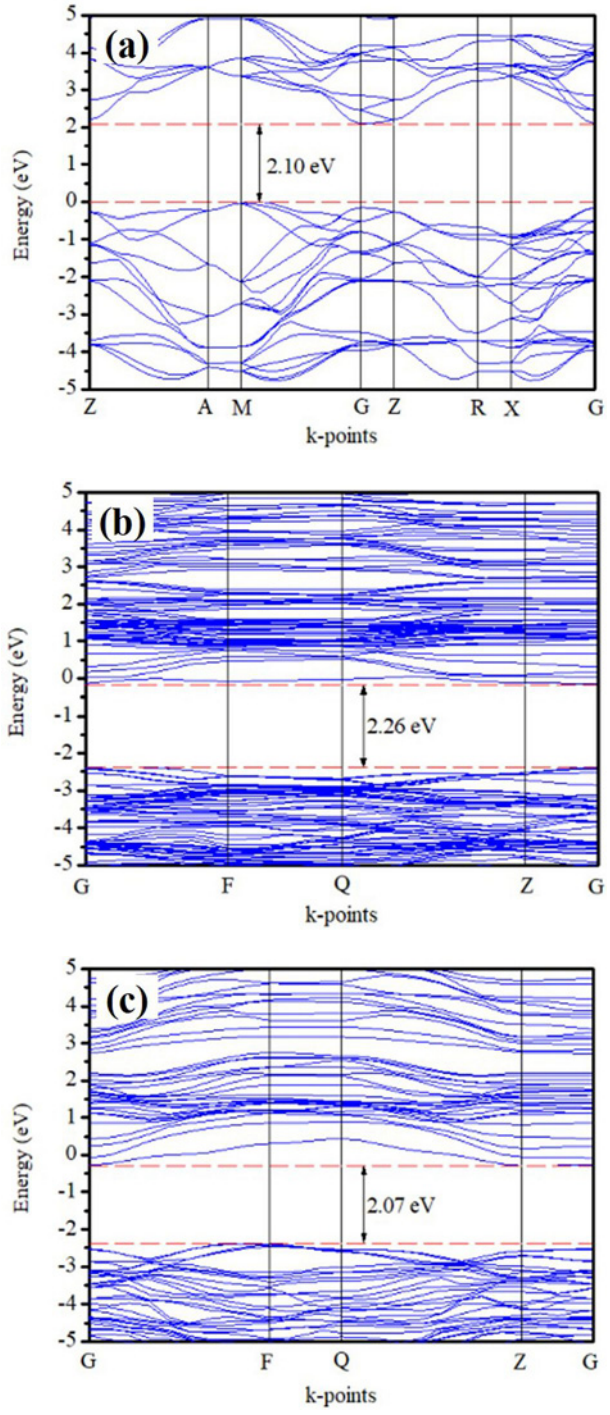

Fig. 2. Calculated band structure of (a) pure TiO_2, (b) 2.08 % As-doped TiO_2, and (c) 4.17 % As-doped TiO_2.

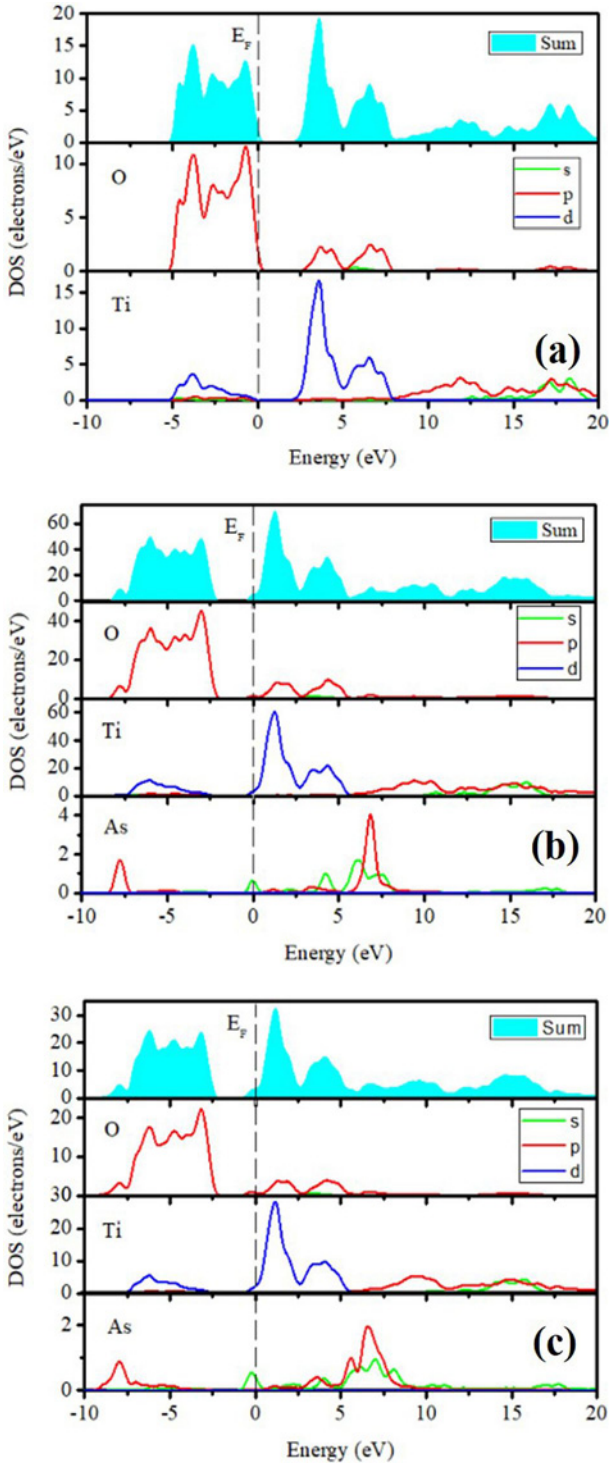

Fig. 3. Calculated DOS of (a) pure TiO_2, (b) 2.08 % As-doped TiO_2, and (c) 4.17 % As-doped TiO_2.

of the valence band and the minimum of the conduction band remains greater than the bandgap energy of pure TiO_2, which is not conducive to subsequent electron migration.

Figure 3c shows the DOS distribution of the 4.17 % As-doped TiO_2. It can be observed that the peak positions of the DOS for each element have not changed significantly. However, due to the relative decrease in the content of O and Ti elements, the heights of the peaks for O and Ti elements start to decrease. With the relatively high content of the As element, its influence is strengthened. It is found that the minimum of

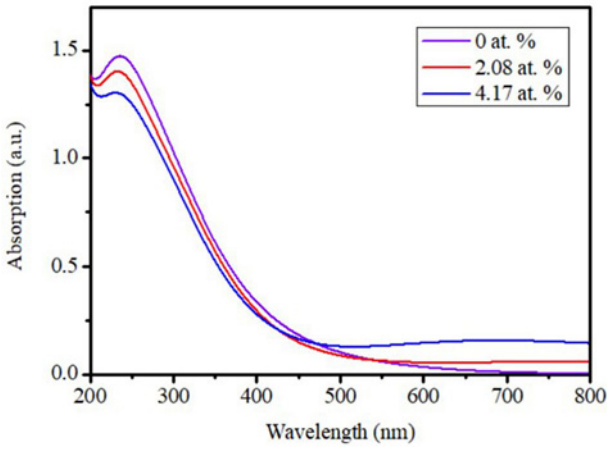

Fig. 4. Calculated absorption of As-doped TiO_2.

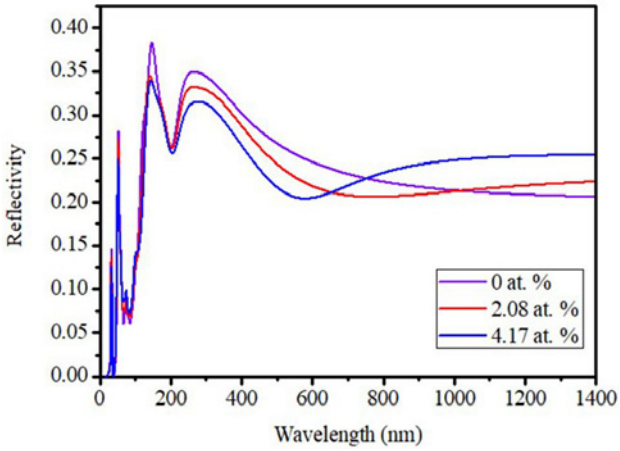

Fig. 5. Calculated reflectivity of As-doped TiO_2.

the conduction band of As-4p further shifts to –0.8 eV, while the maximum of the valence band remains unchanged, resulting in a reduction in the band gap.

3.2. Optical properties

The band gap directly affects the material's light absorption performance, as shown in Fig. 4 for the light absorption spectra of the three models. Pure TiO_2 exhibits strong absorption in the ultraviolet region (< 380 nm) but has minimal absorption in the visible light region (380–780 nm), with only a certain absorption intensity occurring at wavelengths less than 590 nm. Electrons undergo transition after absorbing photons, initiating the absorption of light waves. The relationship between the energy E_g of electron transition across the band gap and the wave-length λ is shown in Eq. (1) [26]:

$$E_g = \frac{1240}{\lambda}. \quad (1)$$

The calculated results indicate that the band gap of pure TiO_2 is 2.10 eV. According to Eq. (1), only wavelengths less than 591 nm may be absorbed by the material. After doping with As, the absorption intensity in the visible light range increases. When the As doping content is at 2.08 %, the change is not significant. However, when the As content reaches 4.17 %, the absorption intensity in the visible light range starts to increase, notably higher than 2.08 % As-doped TiO_2 and pure TiO_2, especially reaching a higher value near 700 nm (1.17 eV). This trend is consistent with the previously mentioned band structure calculation results. The reason is that the band gap of 4.17 % As-doped TiO_2 is minimized to 2.08 eV, which is favorable for the absorption of light by valence band electrons and the realization of transitions to the conduction band.

There is a clear correspondence between the reflectivity and absorption. Figure 5 shows the reflectivity curves of three models. It can be seen that, as the wavelength increases, the trend of reflectivity is similar to the absorption trend (Fig. 4). The three models exhibit essentially the same variation trend in the ultraviolet region. At 145 nm, the reflectivity of pure TiO_2, 2.08 % As-doped TiO_2, and 4.17 % As-doped TiO_2 models reach their highest values, which are 0.38, 0.35, and 0.34, respectively. After that, it decreases, then rises again at 204 nm, reaching a secondary peak at 262 nm. In the visible light region, the reflectivity of the three models decreases as the wavelength increases. The 4.17 % As-doped TiO_2 exhibits a lower reflectance, reaching the minimum at 600 nm, and then begins to increase. Upon entering the infrared region, the reflectivity of the 4.17 % As-doped TiO_2 becomes the highest, reaching above 0.25.

The loss function spectrum describes the energy loss of electrons when rapidly traversing through a material. The loss function value of pure TiO_2 decreases as the wavelength increases (as shown in Fig. 6). After doping with As elements, the loss function value undergoes significant changes in the visible light range (1.58–3.25 eV), with a small peak appearing around 1.7 eV, followed by a decrease. Figure 6 shows that all three models exhibit higher peaks in the 10.5–12.5 eV range, with the peak heights decreasing as the doping content increases.

At the peak, when the real part of the dielectric function reaches zero, it indicates a transition from metallic to dielectric behavior, characterizing the plasmon resonance. The peak position corresponds to the relevant plasmon frequency, a metal characteristic [27]. Combining Figs. 6 and 7, it can be concluded that the plasmon frequencies of pure TiO_2, 2.08 % As-doped TiO_2, and 4.17 % As-doped TiO_2 are 11.36 eV, 10.97 eV, and 10.53 eV, respectively. The

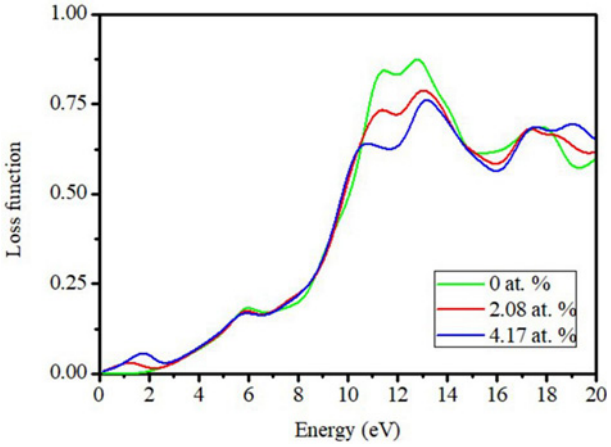

Fig. 6. Calculated loss function of As-doped TiO_2.

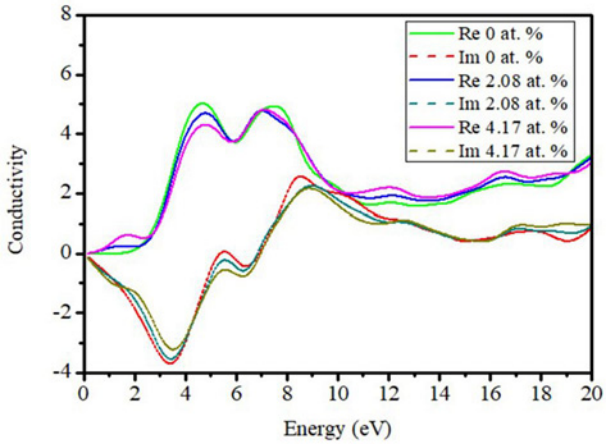

Fig. 8. Calculated conductivity of As-doped TiO_2.

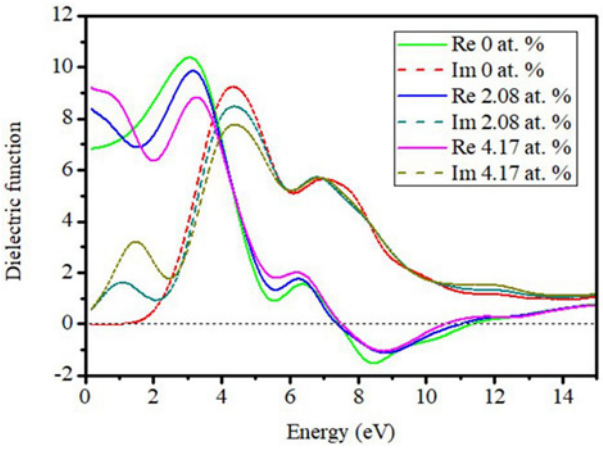

Fig. 7. Calculated dielectric function of As-doped TiO_2.

results indicate that after As doping, the plasmon frequency begins to decrease and gradually decreases with increasing doping content.

Figure 7 shows the dielectric function curves of three models. The solid lines represent the changes in the real part of the function, while the dashed lines represent the changes in the imaginary part. The vertical axis represents the static dielectric constant, reflecting the material's polarization ability under an external electric field. The figure displays the variation of the static dielectric constants for the three models: pure TiO_2 is 6.81, 2.08 % As-doped TiO_2 is 8.37, and 4.17 % As-doped TiO_2 is 9.20. The results indicate that the static dielectric constant begins to increase after As doping, indicating a stronger binding charge capability. From the changes in the imaginary part of the figure, it can be seen that all three models exhibit the highest peak at 4.32 eV and a secondary peak at 6.9 eV. These peaks originate from the electron transitions between Ti-3d, O-2p, As-4s, and As-3p, and their intensity decreases with higher doping content. 2.08 % As-doped TiO_2 exhibits a peak near 1.1 eV in the infrared region. Within the visible light range (1.58–3.25 eV), only the 4.17 % As-doped TiO_2 exhibits a peak near 1.6 eV, indicating an increase in the probability of electron-photon absorption and an increase in the number of excited state electrons, thereby enhancing the probability of subsequent transitions, which is beneficial for the material's application in the visible light range.

Similarly, the changing trend of the imaginary part of the above-mentioned dielectric function is similar to the real part of the conductivity, representing energy dissipation. As shown in Fig. 8, the conductivity of pure TiO_2 has a significant peak in the ultraviolet region, while As-doped TiO_2 shows a decrease in the peak in this region. Only the 4.17 % As-doped TiO_2 shows a weak peak in the region where visible light and ultraviolet light intersect. This indicates that the conductivity in the visible light range can be enhanced after As doping.

4. Conclusions

This paper first used first-principles calculations to study the band structure, atomic state density distribution, absorption, reflectivity, and dielectric function of As-doped TiO_2. The results show that compared to pure TiO_2, the As-4s and As-4p orbitals of As-doped TiO_2 widen the positions of the conduction band minimum and valence band maximum. Additionally, with an increase in As doping, the band gap of the 4.17 % As-doped TiO_2 begins to decrease, lowering the energy required for electron transitions from the valence band to the conduction band and enhancing the absorption in the visible light range. As-doped TiO_2 exhibits excellent reflectivity, dielectric function, and conductivity performance, making it a promising material for photocatalytic applications under visible

light and laying a theoretical foundation for future experimental applications.

References

[1] J. Ma, L. Zhang, Z. Fan, S. Sun, Z. Feng, W. Li, H. Ding, Construction of R-TiO_2/n-TiO_2 heterophase photocatalysts for efficient degradation of organic pollutants, J. Alloys Comp. 968 (2023) 172127. https://doi.org/10.1016/j.jallcom.2023.172127

[2] K. Bommavaram, F. M. Ali, H. Ibrahim, Degradation of wastewater from carbon capture plants using metal-impregnated TiO_2 photocatalyst, Can. J. Chem. Eng. 101 (2023) 6827–6844. https://doi.org/10.1002/cjce.24945

[3] A. Sinhmar, H. Setia, V. Kumar, A. Sobti, A. P. Toor, Enhanced photocatalytic activity of nickel and nitrogen codoped TiO_2 under sunlight, Environ. Technol. Inno. 18 (2020) 100658. https://doi.org/10.1016/j.eti.2020.100658

[4] B. Zhang, H. Wang, J. Luo, S. Liu, Y. Tian, Anatase W-doped TiO_2 nanocrystals with improved Mg^{2+}-excited electrochromic properties, J. Electroanal. Chem. 930 (2023) 117159. https://doi.org/10.1016/j.jelechem.2023.117159

[5] Y. Mingmongkol, D. T. T. Trinh, P. Phuinthiang, D. Channei, K. Ratananikom, A. Nakaruk, W. Khanitchaidecha, Enhanced photocatalytic and photokilling activities of Cu-doped TiO_2 nanoparticles, Nanomaterials 12 (2022) 1198. https://doi.org/ 10.3390/nano12071198

[6] J. H. Luo, Preparation of rare earth Lu-doped TiO_2 film by sol-gel method and its photocatalytic degradation of methyl orange under natural light, Mater. Sci. – Electronic and Optical Materials 28 (2022) 383–387. https://dx.doi.org/ 10.5755/j02.ms.29676

[7] O. A. Osin, T. Yu, X. Cai, Y. Jiang, G. Peng, X. Cheng, R. Li, Y. Qin, S. Lin, Photocatalytic degradation of 4-nitrophenol by C, N-TiO_2: Degradation efficiency vs. embryonic toxicity of the resulting compounds, Front. Chem. 6 (2018) 192. https://doi.org/10.3389/fchem.2018.00192

[8] H. Mandor, N. K. Amin, O. Abdelwahab, E. Z. El-Ashtoukhy, Preparation and characterization of N-doped ZnO and N-doped TiO_2 beads for photocatalytic degradation of phenol and ammonia, Environ. Sci. Pollut. R. 29 (2022) 56845–56862. https://doi.org/10.1007/s11356-022-19421-6

[9] M. Chen, K. Zhuang, J. Sui, C. Sun, Y. Song, N. Jin, Hydrodynamic cavitation-enhanced photocatalytic activity of P-doped TiO_2 for degradation of ciprofloxacin: Synergetic effect and mechanism, Ultrason. Sonochem. 92 (2023) 106265. https://doi.org/10.1016/j.ultsonch.2022.106265

[10] R. Sultana, S. I. Liba, M. A. Rahman, N. Yeachin, I. M. Syed, M. A. Bhuiyan, Enhanced photocatalytic activity in RhB dye degradation by Mn and B co-doped mixed phase TiO_2 photocatalyst under visible light irradiation, Surf. Interfaces 42 (2023) 103302. https://doi.org/10.1016/j.surfin.2023.103302

[11] H. Xing, L. Wu, X. Li, Zn/N co-doped TiO_2 nanotubes for enhancement of photocatalytic degradation of pentachlorophenol, Int. J. Electrochem. Sci. 17 (2022) 22066. https://doi.org/10.20964/2022.05.32

[12] K. P. Suwondo, N. H. Aprilita, E. T. Wahyuni, Enhancement of TiO_2 photocatalytic activity under visible light by doping with Cu from electroplating wastewater, Reac. Kinet. Mech. Cat. 135 (2022) 479–497. https://doi.org/10.1007/s11144-021-02134-1

[13] M. G. Bhosale, R. S. Sutar, S. B. Deshmukh, M. K. Patil, Photocatalytic efficiency of sol-gel synthesized Mn-doped TiO_2 nanoparticles for degradation of brilliant green dye and mixture of dyes, J. Chin. Chem. Soc. 69 (2022) 1730–1743. https://doi.org/10.1002/jccs.202200248

[14] Y. E. Durmus, C. Roitzheim, H. Tempel, F. Hausen, Y. Ein-Eli, H. Kungl, R.-A. Eichel, Analysis on discharge behavior and performance of As- and B-doped silicon anodes in non-aqueous Si-air batteries under pulsed discharge operation, J. Appl. Electrochem. 50 (2020) 93–109. https://doi.org/10.1007/s10800-019-01372-5

[15] S. Sen, D. Acharya, P. K. Guha, P. Banerji, P. Pramanik, Comprehensive electrical characterization and theoretical analysis of Mn and As doped β-$FeSi_2$ through DFT: A promise to rectification and photovoltaic applications, J. Appl. Phys. 134 (2023) 025702. https://doi.org/10.1063/5.0149138

[16] C. Jiang, E. Colegrove, S. P. Harvey, J. N. Duenow, E. Sartor, M. O. Reese, Nanometer-scale electrical potential imaging on absorber of CdSeTe solar cells, Sol. Energ. Mater. Sol. C. 260 (2023) 112465. https://doi.org/10.1016/j.solmat.2023.112465

[17] Y. Zhao, Y. Sun, Z. Guo, J. Qiu, X. Sun, First-principles investigations of arsenate doping into the ettringite lattice, J. Clean. Prod. 419 (2023) 138266. https://doi.org/10.1016/j.jclepro.2023.138266

[18] J. H. Luo, L. J. Xiang, L. S. Chen, Y. Li, First-principle study on the optical properties of TiO_2 doped with different Lu contents, J. Ovonic Res. 19 (2023) 775–782. https://doi.org/10.15251/JOR.2023.196.775

[19] V. Christhunathan, P. Farrès, M. Tong, First-principles study of electronic properties of Zn and La doped and co-doped anatase TiO_2, AIP Adv. 13 (2023) 125013. https://doi.org/10.1063/5.0174393

[20] A. Y. Yu, Q. M. Hu, R. Yang, First-principles investigation of alloying elements on Ti/TiO_2 interface, Kovove Mater. 55 (2017) 291–294. https://doi.org/10.4149/km_2017_4_291

[21] M. C. Payne, M. P. Teter, D. C. Allan, T. A. Arias, J. D. Joannopoulos, Iterative minimization techniques for ab initio total-energy calculations: Molecular dynamics and conjugate gradients, Rev. Mod. Phys. 64 (1992) 1045–1097. https://doi.org/10.1103/RevModPhys.64.1045

[22] B. Hammer, L. B. Hansen, J. K. Nørskov, Improved adsorption energetics within density-functional theory using revised Perdew-Burke-Ernzerhof functionals, Phys. Rev. B 59 (1999) 7413. https://doi.org/10.1103/PhysRevB.59.7413

[23] Z. Zeng, M. Xu, Y. Sun, J. Xu, Y. Zhong, First-principles study on the optical spectrum of N/P doped TiO_2-anatase, Optik 261 (2022) 169231. https://doi.org/10.1016/j.ijleo.2022.169231

[24] M. Khan, J. Xu, N. Chen, W. Cao, First principle calculations of the electronic and optical properties of pure and (Mo, N) co-doped anatase TiO_2, J. Alloy Compd. 513 (2012) 539–545. https://doi.org/10.1016/j.jallcom.2011.11.002

[25] S. Liu, B. Liu, T. Wang, S. Zhu, Y. Li, High anisotropic magnetoresistance, perfect spin-filtering effect, and negative differential resistance effect of Cr-doped anatase phase TiO_2, Phys. Scr. 98 (2023) 015827. https://doi.org/10.1088/1402-4896/acaa74

[26] P. Ji, J. Zhang, F. Chen, M. Anpo, Ordered mesoporous CeO_2 synthesized by nanocasting from cubic Ia3d mesoporous MCM-48 Silica: Formation, characterization and photocatalytic activity, J. Phys. Chem. C 112 (2008) 17809–17813. https://doi.org/10.1021/jp8054087

[27] L. Xiao, Y. Su, X. Zhou, H. Chen, J. Tan, T. Hu, J. Yan, P. Peng, Origins of high visible light transparency and solar heat-shielding performance in LaB6, Appl. Phys. Lett. 101 (2012) 041913. https://doi.org/10.1063/1.4733386